iScience

CellPress
OPEN ACCESS

Article

Investigation of synergic effects of nanogroove topography and polyaniline-chitosan nanocomposites on PC12 cell differentiation and axonogenesis

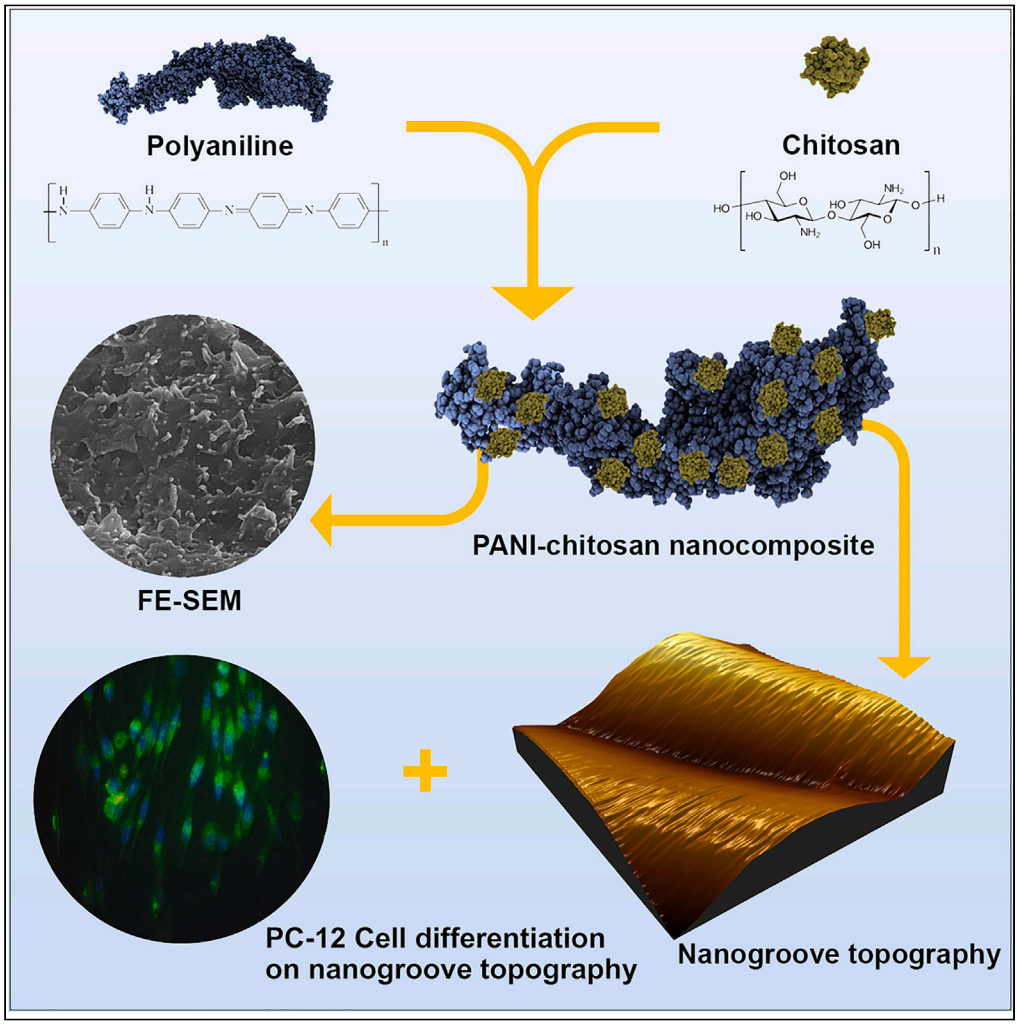

Mohammad Hossein Afsharian, Reza Mahdavian, Samira Jafari, Abdollah Allahverdi, Hossein Soleymani, Hossein Naderi-Manesh

a-allahverdi@modares.ac.ir

Highlights

Nanogroove topography can induce cell alignment parallel to the direction of grooves

The presence of chitosan can improve the physicochemical properties of nanosubstrates

The use of nanocomposite and topography led to the differentiation of somatic cells

Afsharian et al., iScience 27, 108828
February 16, 2024
https://doi.org/10.1016/j.isci.2024.108828

iScience

CellPress
OPEN ACCESS

Article

Investigation of synergic effects of nanogroove topography and polyaniline-chitosan nanocomposites on PC12 cell differentiation and axonogenesis

Mohammad Hossein Afsharian,[1] Reza Mahdavian,[1] Samira Jafari,[2] Abdollah Allahverdi,[1,3,*] Hossein Soleymani,[1] and Hossein Naderi-Manesh[1]

SUMMARY

Axonal damage is the main characteristic of neurodegenerative diseases. This research was focused on remodeling cell morphology and developing a semi-tissue nanoenvironment via mechanobiological stimuli. The combination of nanogroove topography and polyaniline-chitosan enabled the manipulation of the cells by changing the morphology of PC12 cells to spindle shape and inducing the early stage of signal transduction, which is vital for differentiation. The nanosubstarte embedded with nanogooves induced PC12 cells to elongate their morphology and increase their size by 51% as compared with controls. In addition, the use of an electroconductive nanocomposite alongside nanogrooves resulted in the differentiation of PC12 cells into neurons with an average length of 193 $\pm$7 μm for each axon and an average number of seven axons for each neurite. Our results represent a combined tool to initiate a promising future for cell reprogramming by inducing cell differentiation and specific cellular morphology in many cases, including neurodegenerative diseases.

INTRODUCTION

Every year, thousands of deaths and disabilities are recorded worldwide due to neuronal diseases. Among the various types of diseases, neurodegenerative diseases are the most complicated. This class of diseases includes Alzheimer's disease, Parkinson's disease, Huntington's disease, Friedreich's ataxia, and amyotrophic lateral sclerosis (ALS). Because current understandings do not elucidate all aspects of the diseases, their condition deteriorates during the diagnosis and treatment procedures. According to the global burden of diseases (GBD), neurological disorders came in second, accounting for 11.6% of global mortality, trailing only cardiovascular diseases, which accounted for 16.5%.[1] There are many concerning cellular factors in neurodegenerative diseases. One of the main pathological symptoms is known as "dying-back" degeneration, which is due to metabolic failure at the presynaptic terminal.[2] Recent material science and tissue engineering advances have led to bio-friendly materials with myriad applications.[3] Hence, it is now common to use biodegradable synthetic polymers, including single-walled carbon nanotubes (SWNTs), polycaprolactone (PCL), polydimethylsiloxane (PDMS), and polyhydroxybutyrate, in association with chitosan, laminin, collagen, and alginate.[4–9] Although many studies have focused on the chemical and molecular factors that cause these diseases, new findings suggest mechanical and nanotopographical stimuli play important roles as well. In general, cells can sense environmental stimuli, such as nanoscale topographic cues embedded in their microenvironment, alongside chemical and molecular cues. In more detail, cell proliferation, cell adhesion, cell differentiation, and axonogenesis can be affected by nanosubstrates embedded with nanotopography cues.[9–12] Fundamental studies have shown that cellular sensing of nanotopography is critically dependent on the attachment of membrane molecules such as integrins and extracellular nanotopographic features.[13,14] Notably, through different types of nanotopographies, nanogrooves appear to be a strong factor in triggering the initial differentiation of neurons and advancing stages of differentiation, such as axonogenesis. Significantly, PDMS nanogrooves can enhance neurite outgrowth and cell alignment in 3D culture.[15] Furthermore, the biocompatibility, versatility, rubber- such as elastic properties, and transparency of PDMS, besides the importance of nanotopography and its intrinsic effects on cell fate, represent a strong tool in cell studies. PDMS works as a suitable implant when combined with hydroxyapatite, alginate, and collagen. This implant can initiate neurogenesis by suppressing inflammation with amino acids as crosslinks.[16] Electroconductive materials such as polyaniline (PANI), polypyrrole (PPy), poly (3,4- ethylenedioxythiophene) (PEDOT), and graphite derivatives such as graphene oxide (GO) and graphene quantum dots (GQDs) work as the best candidates for studying cellular behavior in neurons.[15,17–19] As a result of its biocompatibility and low cytotoxicity, PANI appears to be a suitable electroconductive material for studying neuronal behaviors in both single-cell and tissue stages.[20–22] As a comparison, it is reported that PANI shows more toxicity under the same conditions than its "base vs. salt"

[1]Department of Biophysics, Faculty of Biological Sciences Tarbiat Modares University, Jalal Ale Ahmad Highway, P.O. Box: 14115-111, Tehran, Iran
[2]Pharmaceutical Sciences Research Center, School of Pharmacy, Kermanshah University of Medical Sciences, Kermanshah, Iran
[3]Lead contact
*Correspondence: a-allahverdi@modares.ac.ir
https://doi.org/10.1016/j.isci.2024.108828

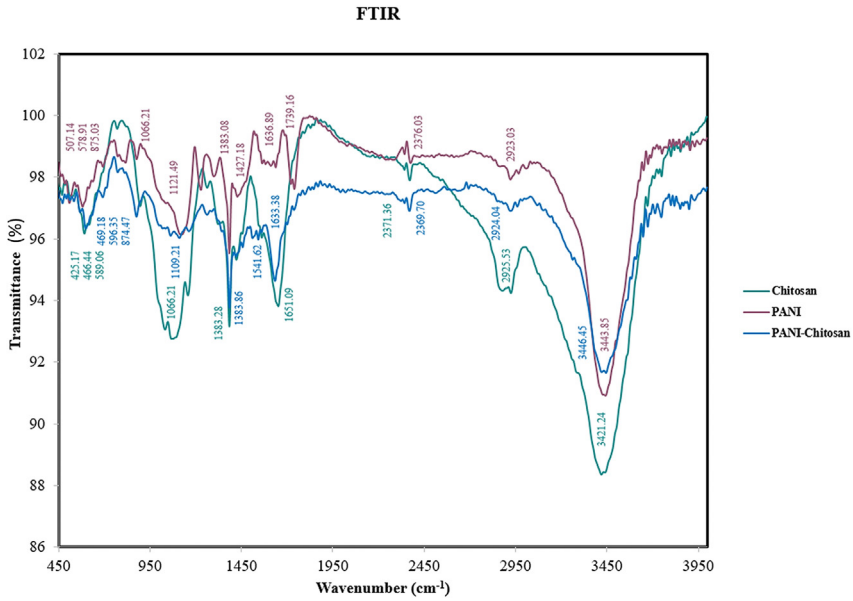

Figure 1. The FTIR spectra of PANI, chitosan, and PANI-C

form.[22] Among different natural biopolymers, chitosan represents numerous advantages, including antibacterial properties, hydrophilicity, and biocompatibility. Interestingly, chemical modifications to synthesize bio-nanocomposites can easily occur in the backbone of chitosan, which is enriched with hydroxyl and amino groups. Therefore, it is now possible to investigate the features of the cell more deeply by combining the electrical conductivity of PANI with the biological advantages of chitosan.[23–25] In addition to its ability to form nanofilms, Rahman et al. reported that the PANI-chitosan nanocomposite was soluble in polar organic solvents.[25] This type of nanocomposite has a high potential for establishing communication between isolated cells to induce the early stages of histogenesis. The PANI-C nanocomposite was used in drug delivery and enzymology studies, and it can be seen as a nanocarrier for proteins.[26] Rat pheochromocytoma cells are one of the most popular cell models in neuroscience, axonogenesis, and synaptogenesis studies. The polygonal shape of the PC12 cell line is a helpful morphology as compared with their counterparts cultured on nanotopography for visual analysis.[27–29] Although the PC12 cell line originated from the rat adrenal medulla, after treatment with NGF (nerve growth factor), it differentiates into sympathetic ganglion neurons not only morphologically but also functionally.[30,31] In this study, we investigated the effects of both nanotopography and PANI-chitosan nanocomposite on PC12 cell line differentiation into neuron cells. Accordingly, mechanical tests such as AFM and nano-indentation were used to measure the biophysical parameters of the nanosubstrate, such as roughness and Young's modulus. Furthermore, spectroscopic and microscopic techniques were conducted to quantitatively characterize PANI-chitosan nanocomposites (FTIR, XRD, UV-visible, and SEM). Finally, the cytotoxicity of PANI-nanocomposites and the cell differentiation and morphology of the PC12 cell line were investigated through the MTT assay, antibody staining, and fluorescence microscopy. Based on the obtained data, mechanotransduction can play an important role alongside chemical and molecular factors in dictating cells' morphology. Besides, the effects of PANI-chitosan nanocomposites on PC12 cells are undeniable. Significantly, nanotopographies and electroconductive materials can be helpful tools in cell reprogramming. The results of this article suggest that the synergistic effects of nanotopography and nanocomposites can simultaneously target cell differentiation and cell morphology, which are both lost keys in neurodegenerative diseases.

RESULTS

Fourier transform infrared spectra of polyaniline-chitosan

The formation of PANI-C nanocomposite occurred by the transverse conjugation of the -NH_2 and -OH groups of PANI and chitosan.[32] Hence, FTIR spectroscopy was carried out to determine the formation of appeared bonds in the PANI-C nanocomposite. The FT-IR spectra of pure PANI, chitosan, and PANI-C were measured at a wavelength between 400 and 4000 cm^{-1} (Figure 1). The PANI characteristic peaks include broad peaks ranging from 3016 to 3443.85 cm^{-1} corresponding to N–H stretching vibrations of a secondary amine and a sharp peak at 1636.89 cm^{-1} representing C=C stretching of the quinoid ring N = Q = N, peaks at 1383.08 and 1427.18 cm^{-1} representing C=C stretching vibration of the benzenoid ring (N-B-N), 1227.21 and 1298.49 cm^{-1} are accounted for the π-electron delocalization induced in the polymer through protonation in C-N stretching of the secondary aromatic ring, respectively, 1121.49 cm^{-1}, 875.03, 814.27, and 578.91 cm^{-1} are attributed to aromatic C-H in-plane bending vibrations and aromatic C-H out-of-plane bending vibrations. For chitosan, a broad-wide peak was observed at 3151–3421.24 cm^{-1} which represents N-H and O-H stretching as well as the intramolecular hydrogen bonds. The absorption bands at around 2925.53 and 2866 cm^{-1} can be applied to C-H symmetric and asymmetric stretching. Notably, -NH_2 groups were detected

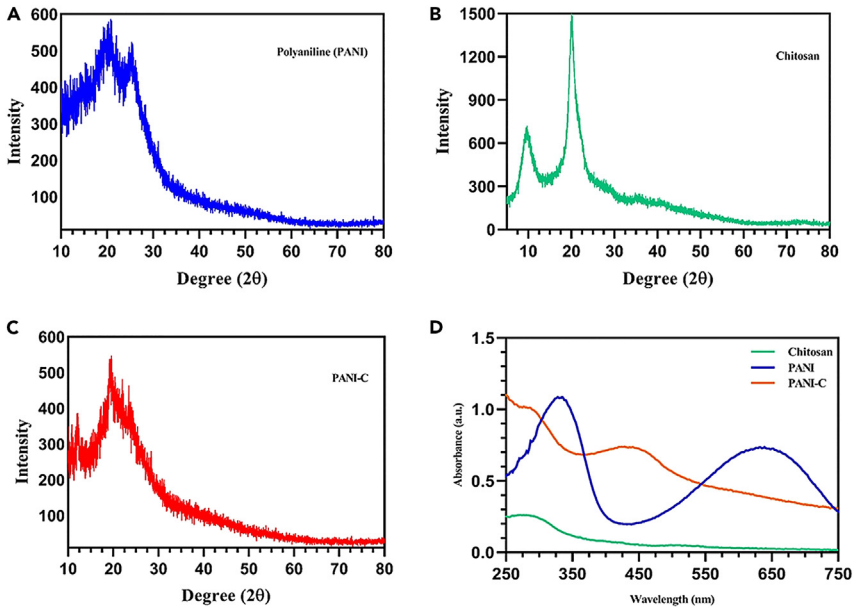

Figure 2. Characterization of PANI, chitosan, and PANI-C using X-ray diffraction and UV-visible spectroscopy

(A) X-ray diffraction of PANI.

(B) X-ray diffraction of chitosan.

(C) X-ray diffraction of PANI-C nanocomposites.

(D) UV-visible spectra of chitosan, PANI, and PANI-C.

at 1651.09 cm^{-1} while there were no peaks of C-N stretching of amide II or C-N stretching of amide III due to possible overlaps with other peaks. The CH_2 bending and CH3 symmetrical deformations were confirmed by the presence of bands at around 1421.55 and 1383 cm^{-1}, respectively. The absorption band at 1156.34 cm^{-1} can be attributed to the asymmetric stretching of the C-*O*-C bridge. The bands at 1040 and 1066 cm^{-1} correspond to C-O stretching. The peaks in PANI-C nanocomposites were described as follows: the broad peak at 3209–3446.45 cm^{-1} describes N-H and O-H stretching vibrations. The peaks at 1383.86 cm^{-1} and 874.47 cm^{-1} can be assigned to C-N stretching of the secondary aromatic amine and aromatic C-H out-of-plane bending vibrations, respectively. A peak at 1633.38 cm^{-1} and 1541.62 cm^{-1} is attributed to N-H bending, while the band at 1480 cm^{-1} represents the C-C aromatic ring stretching of the benzenoid unit, and the vibrations at 1261 cm^{-1} and 1109.21 cm^{-1} are the characteristic vibrations of C-O stretching. The decrease in the intensity of N-H and O-H peaks (3209–3446.45 cm^{-1}) alongside the shifted-decreased peak of N-H (1633.38 cm^{-1}) in PANI-C confirmed the formation of transversal bonds between chitosan and PANI. All of the peak positions are closely related to previous reports.[33–36]

X-Ray diffraction of the nanocomposite

Due to its versatility and non-destructive approach, X-ray diffraction is used to determine phase composition, grain size, crystallinity, and phase. The samples in powder form were analyzed by X-ray diffraction to determine the crystal structure (Figure 2). There are two diffraction peaks at 20.03° and 25.42°. Due to the presence of benzenoid and quinonoid groups, PANI shows a semi-crystalline structure. The XRD spectra of chitosan showed peaks at 10° and 19°, which are consistent with other literature.[37] Notably, the PANI-C XRD pattern shows four peaks, including 12.13°, 19.45°, 21.95°, and 23.93°.[38] The XRD pattern of PANI-C nanocomposites includes both the chitosan and PANI diffraction patterns.

UV-visible spectra of polyaniline-chitosan

The UV spectra of PANI and PANI-C were measured in NMP (N-Methyl-2-pyrrolidone) and acetonitrile, respectively (Figure 2). The UV-vis absorption of PANI is highly dependent on the level of doping, the extent of conjugation, the nature of the polymer, and the solvent. PANI exhibits two major bands: 340–370 nm, and 600–650 nm. Respectively, the first bond around 340–370 nm corresponds to $\pi - \pi^*$ molecular orbital transitions in the aromatic rings, while around 600–650 nm corresponds to $n - \pi^*$ intramolecular electronic transitions between quinoid and benzenoid units.[39] A broad peak was observed for PANI-C nanocomposites around 390–475 nm, beside a peak around 290–320 nm. Auxochrome is a functional group such as -NH_2 and -OH that does not exhibit absobtion in the UV-Vis region, but it leads to a bathochromic shift in chromophore peaks as well as an increase in their intensities. The PANI-C peaks showed both decreased intensity and hypsochromic shift, which is due to the formation of new bonds and a decrease in the population of -NH_2 and -OH groups. All the results are in accordance with other literature.[32,40]

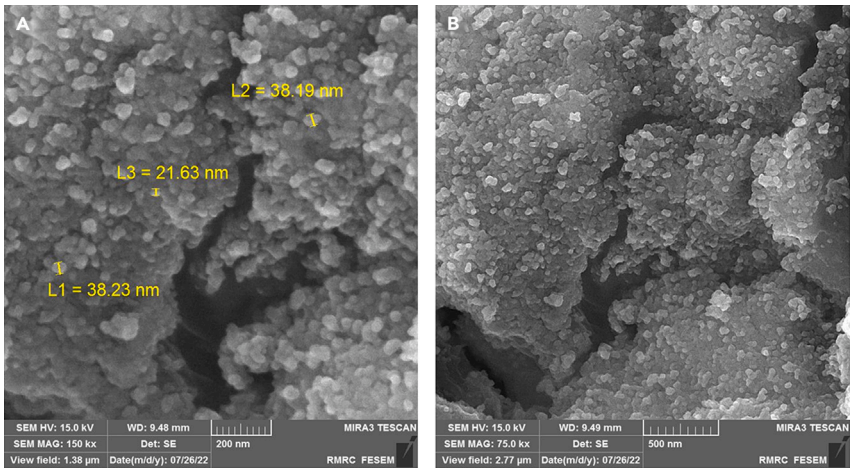

Figure 3. FESEM images of PANI-C molecules

(A) Single PANI-C molecules.

(B) PANI-C populations accumulated as nanoclusters.

FESEM images of polyaniline-chitosan

The morphology of PANI-C nanocomposites was investigated by FESEM (Figure 3) to represent the structure of PANI-C. Single particle analysis shows that PANI-C nanocomposites are in the size range of 21–38 nm and have a spherical structure, while PANI-C particles form nanoclusters in large numbers.

Cytotoxicity assay

An MTT assay was carried out to maintain the PANI and PANI-C cytotoxicity profiles. The result revealed that PANI is a fully biocompatible material, being consistent in low concentrations (30, 60, and 90 μg/mL) while showing mild toxicity in high concentrations (120, 150, and 200 μg/mL) (Figure 4). On the other hand, the assay for PANI-C exhibited the fact that cell proliferation decreased from the lowest concentration to the highest (Figure 4). It is also significant that cell density slightly decreased as the PANI-C concentration increased. There is both molecular and cellular evidence to justify the significant difference between PANI and PANI-C cytotoxicity. The presence of chitosan increases surface hydrophilicity and decreases the possibility of PC12 cells' aggregation by minimizing cell clumps. Unlike cell-substrate interaction, cell aggregation represents strong cell-cell interaction, which is the main cause of growing cell clumps due to cell migration.[41–43] In other words, the combination of chitosan and nanogroove topography can subsequently decrease both the size and the number of cell clumps by altering cell migration and strengthening the cell-substrate interactions.

Visualizing the morphology of cultured cells on nanosubstrate

In order to maintain the initiated morphology, the cells were cultured on flat PDMS as the control and on a PDMS substrate embedded with nanogrooves. As a result, cells cultured on the nanogroove surface displayed a dominant bipolar spindle morphology and were elongated along the direction of the grooves, while cells exhibited random morphology in the control sample (Figure 5). As follows, aligned and control cells exhibit subsequent lengths of 247 ±21 and 163 ±6 μm. The analysis of the morphology proved that PC12 cells increased their length by up to 51% as compared with controls. The elongation of PC12 cells is highly dependent on cell orientation. Hence, the angle of the cells was measured at about 81 ± 4°. The angle confirmed that cell alignment was induced by topography. These results indicate that the topographical cue of nanogrooves plays an important role in cell guidance and cell reprogramming by inducing changes in the nucleus, cell membrane, focal adhesions, and cytoskeleton via nanotopography. Furthermore, SEM images of cells (Figure 6) confirmed the changes in the polygonal shape of PC12 cells to spindle shape after cells were cultured on the nanosubstrate. It is also noticeable that cell-cell interactions are reinforced after the attachment of single cells to nanotopography. The SEM images of cells indicated that the attachment of cells to surfaces was mediated by the expansion of lamellipodia as they aligned toward the direction of nanogrooves, both at the single cell and population levels. Further analysis of the pictures revealed the fact that cells tend to initiate cell-cell interactions via leading filopodia. The formation of cell-cell interaction led to the early stages of axonogenesis by initiating cellular responses via mechanosensing stimuli.

PC12 cell line differentiation to neurons

The nanosubstrate was prepared and coated with PANI-C nanocomposite without any functionalizing attachment factor (laminin, fibronectin, or poly-L-lysine). The PC12 cells were seeded on a nanosubstrate, and the differentiation of PC12 cells into neurons occurred after a 14-day culture on nanogrooves (Figure 7). The positive control (cells treated with NGF) was also performed as a comparison. The cells were then incubated with antibodies against neurofilament 68. The physical contact with the surface, along with the intrinsic properties of PANI-C,

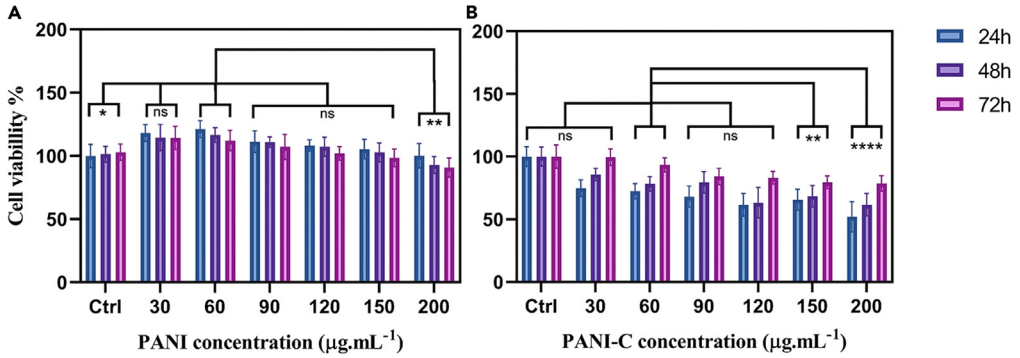

Figure 4. The MTT viability assay of cultured PC12 cells incubated with different concentrations of PANI and PANI-C

(A) Various concentrations of PANI.

(B) Various concentrations of PANI-C.

induced the formation of neurites with several axons. The accumulation of neurofilaments is greatest around the nuclei, which might be due to the self-assembly of nuclei under the effect of nanotopography. Therefore, the investigation of the neurons indicated that, on average, each neurite grew seven axons with an average length of 193 ±7 μm. Recent studies reported that nanogroove topography initiates the activation of MAPK/ERK downstream and increases the expression of β-III-tubulin as a specific neuronal marker.[44,45] In addition, slight differences in the width of the ridge of nanogrooves can simply change the neurite angle of cells.

Characterization of mechanical properties by nanoindentation

Mechanical tests were obtained by the penetration of a sharp indenter into the surface of PDMS (10:1) (Figure 8). The Young's modulus parameters for PDMS, PDMS-PANI, and PDMS-PANI-C were subsequently determined to be, respectively, 393 ± 66, 394 ± 76, and 320 ± 86 MPa. It was reported that the Young's modulus of PDMS is highly dependent on the thickness of the substrate and the weight ratio of the curing agent. Hence, the softer the PDMS nanosubstrate, the higher the weight ratio.[46] Previous studies reported that Young's modulus of PANI is dependent on pressure; as it goes up from 300 to 800 MPa, the sample becomes brittle.[47] The measured Young's modulus for PANI, which was coated on a PDMS substrate, indicates the range of the nanoparticle in the elastic zone. Although, based on statistical analysis, there was no significant difference between the Young's modulus of PDMS and PDMS-PANI, the parameter decreased with the presence of chitosan in PDMS-PANI-C. This is basically because several factors, such as the type of acid dopant and the time of doping, initiate the hydrolysis of chitosan, which acts as the matrix of the nanosubstrate.[46,48] Based on reports, it is also considerable that the time of doping affects the formation of nanocomposites with a more crystalline structure, which leads to brittle samples.[48] Hence, the decrease in Young's modulus of PDMS-PANI-C as compared with PDMS and PDMS-PANI is perhaps related to the fact above (Figure S1). Subsequently, the stiffness of the samples was measured. The parameter for PDMS was measured at about 0.70 μN/nm while there was a mild increase up to 0.76 μN/ nm for PDMS-PANI, which is due to the nature of the PANI nanoparticles that were coated on the substrate. Notably, after the addition of chitosan to the nanoparticle, the stiffness showed a sudden decrease to 0.49 μN/nm; this may be related to the fact that the PANI-C nanoparticle is more fragile as compared with the PANI, so due to the incomplete viscoelastic recovery, it exhibited lower stiffness (Figure S1). Unlike the stiffness, the hardness of PDMS (208 ± 30 nm) and PDMS-PANI-C (201 ± 37 nm) remained unchanged without any significant changes, but the hardness increased for PDMS-PANI (244 ± 44 nm). The increased hardness of PDMS-PANI is perhaps because of the thin layer of PANI nanoparticles that were coated on PDMS, whereas PANI-C was less resistant against tensile strength due to the crosslinks of chitosan.

Atomic force microscopy assay of the nanosubstrate

To determine the fidelity of the existing nanogroove topography, an AFM assay of the samples, including smooth PDMS and PDMS embedded with nanogrooves and coated PANI-C nanocomposites (Figure 9), was carried out. The AFM analysis revealed the nanotopographies of a repeating parallel groove in stretched PDMS sheets, while there was no sign of nanogroove topographies on flat PDMS. In particular, the width of the ridge of nanogrooves was discovered to be approximately 125 ± 94 nm. The surface roughness of the flat PDMS and nanogrooved PDMS was measured. The roughness of the flat used as the control was 20 ± 2 nm, while the amount for the PDMS embedded with nanogrooves increased up to 25±4 nm, which is due to the protrusions that are related to the presence of the nanotopographies. It is also significant that nanogrooved PDMS showed a decrease (12 ± 1 nm) in the roughness parameter after the treatment with PANI-C nanoparticles, which is basically because nanoparticles formed a single-thin monolayer on the nanosubstrate and filled the gaps.

DISCUSSION

It plays a key role in modulating neuronal regeneration and axonogenesis by shortening the nerve repair time, which can be realized by pathological symptoms including rapidly eliminating inflammation, enhancing angiogenesis, promoting proliferation, and promoting migration.[49] In addition, the remodeling of the extracellular matrix (ECM) plays an important role in cell regeneration, as it leads to the secretion of

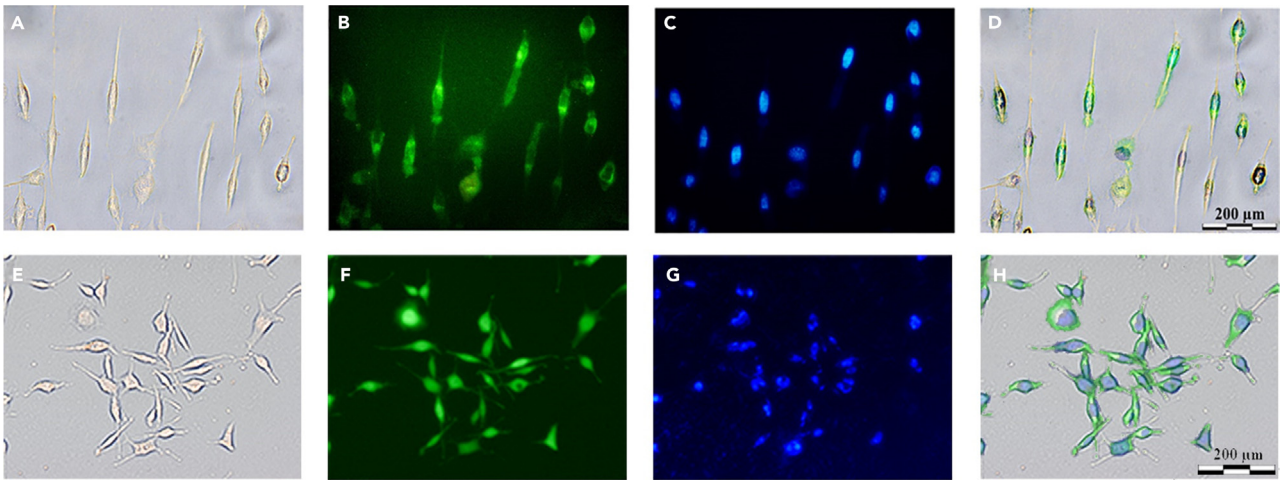

Figure 5. The microscopic images of PC12 cell line morphology before and after the alignment in the direction of the nanogrooves

(A) phase contrast.
(B) Cytoplasm stained by Calcein AM.
(C) nucleus stained by Hoechst.
(D) The merging of phase contrast and fluorescent images.
(E) The phase contrast of the control group.
(F) Cytoplasm of the control group stained by Calcein AM.
(G) Nucleus of the control group stained by Hoechst.
(H) The merged phase contrast and fluorescent images of the control group.

neurotrophic factors such as NGF to accelerate the extension of axons. Regarding the fact that neurons are electrically active, electrical signals can provide stimulation for nerve connectivity and cell growth to improve nerve regeneration. Recent studies showed that by applying external electrical signals, axon extension was promoted. In the presence of nanoparticles featuring biological effectors such as chitosan, cells can trigger the release of NGF, accelerating neurite extension and providing an ideal microenvironment.[49] Numerous studies have indicated the effect of nanotopography on different aspects of cells, such as cell adhesion and cell differentiation. Among different types of nanotopographies, nanogroove topography has been widely used to initiate cell alignment and polarize different neural models.[15,50,51] It was shown that SWNT as single nanotopographic units formed *meta*-nanotopographic structures described as bundled SWNTs that initiate neuronal differentiation by triggering TrkB dimerization and autophosphorylation, which results in the activation of downstream signaling pathways including the PI3K/Akt and MAPK pathways.[4] Besides, electroconductive materials such as polyaniline induce cellular plasticity and differentiation by initiating biophysical cues including axonal guidance, nerve growth, and membrane depolarization of neurons in the regeneration process.[27,52] Nevertheless, due to the weak hydrophilicity of nanosubstartes, blending polymers with biomaterials such as chitosan is necessary. This strategy provided an opportunity to enhance cell attachment by trapping cells in nanogrooves (physically) and increasing the hydrophilicity of nanosubstrates (chemically). In addition, the plasma treatment of nanosubstrate before the coating of PANI-C nanocomposites reinforced the physicochemical properties of the surface by introducing polar functional hydroxyl(-OH) groups, which led to enhanced hydrophilicity.[38] Therefore, the nanosubstrate with PANI-C shares biocompatible, biodegradable, non-immunogenic, antibacterial, and electrical properties, in addition to reinforced mechanical properties.[53,54] This research indicated that the anisotrophic nature of nanogroove topography, regardless of substrate dimensionality, dictates the neurofilament assembly required for directed cell differentiation by changing cells' morphology. Cells in a non-aligned state possess multidirectional protrusions, which result in random cell attachment and cell migration. In contrast, cells in an aligned state possess fewer protrusions and random attachments; during cell alignment, protrusions are limited to a small amount in the direction of nanogroove topography and lead to reinforced cell adhesion and reduced cell migration. This suggests that cell alignment affects the number and location of active protrusions by mimicking multidirectional protrusions and applying uniaxial directional protrusions to the aligned cells. The cell alignment becomes stronger as cells are cultured on smaller-scale topographies. It was reported that cells were oriented at a degree of 10° while cells were cultured on microtopographies, while in this work, cells were oriented at 81 $\pm$ 4° after they were cultured on nanogroove topography (ridge width of 125 $\pm$ 94 nm).[55] The nanopatterned surfaces with smaller nanogrooves provided sharper cell alignment parallel to the nanotopogarphy direction.[55] The chemical modification of the surface, in addition to the physical role of the fabricated nanogrooves, acts as simultaneous factors that allow cells to interact with receptor proteins on the cell surface, which can mediate the molecular pathways leading to growth arrest and the initiation of differentiation. While differentiated neurites have an average of 7 axons, there is a strong correlation between axonal growth and (Figure S2). The physical characteristics of nanotopogarphy, such as height or width, have effects on axonogenesis behavior, including turning, branching, and alignment.[44,56] Axons in microscale topography exhibit less branching, greater alignment, and longer growth, whereas nanoscale topography stimulates the branching level and the number of axons.[56,57] Significantly, the height of the nanogroove topography has an impact on axonal growth. In the case of a low height (26 nm),

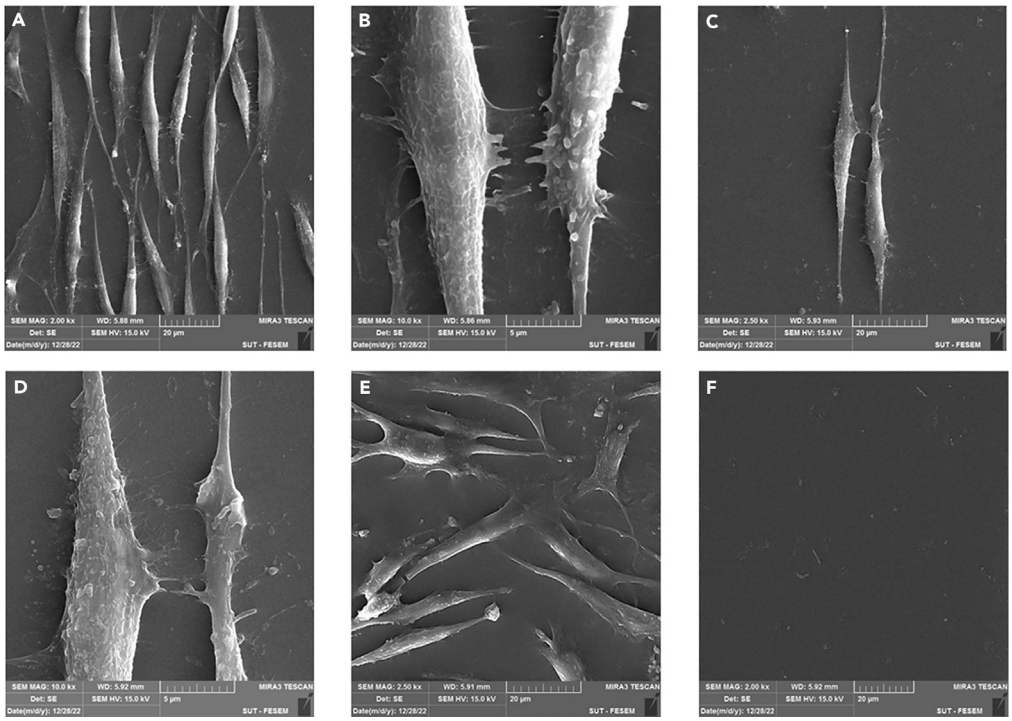

Figure 6. FESEM images of cells cultured on nanogroove topography

(A) The morphology of the cells beside filopodia and cell-cell interactions.

(B) The early formation of axons in cells.

(C) Single cells cultured on nanogroove topography.

(D) The early formation of axons in a single cell.

(E) Random direction of a positive control group of cells in bulk level.

(F) SEM image of bare nanosubstrate.

neurites tend to form and outgrow axons regardless of the patterned surface, while they form aligned axons toward the direction of nanogrooves at high heights (>130 nm).[58] Due to the height of our fabricated nanosubstarte (v) differentiated neurons extend short-range axonal webs with a high level of branching. It was suggested that the differentiation of PC12 cells is mediated by the MAPK/ERK (mitogen-activated protein kinases/extracellular signal-regulated kinases) pathway.[27,43] Yet the molecular mechanism behind the differentiation of neurons via mechanosensing is not clear. Wiatrak et al. showed that the PC12 cell line is responsive to NGF treatment and starts growing neurites at the early stage of axonogenesis, regardless of NGF origin.[29] The combination of PANI-C nanocomposites and nanogroove topography initiates the ability to release neurotrophic factors such as nerve growth factor (NGF) in PC12 cells, which provides neuronal differentiation. Hence, it justifies the fact that cells cultured on plain PANI-C nanocomposites showed less differentiation than cells cultured on PANI-C nanocomposites embedded with nanogroove topography (Figure S2). The changes in cell morphology and increase in neurite outgrowth suggest both nanotopography and nanocomposites appeared as supportive stimuli in the process of PC12 differentiation.

Conclusions

Axonal damage is the main symptom of neurodegenerative diseases. In this work, we have differentiated the PC12 cell line into neuron cells using nanogroove topography and PANI-C nanocomposite. The electroconductivity of PANI can mimic the electrical conductivity of cells and result in axonogenesis by altering membrane depolarization and the initiation of cell responses. This simply induced neurogenesis and axon guidance through the involvement of endogenous electrical signals. The presence of chitosan improved the mechanical properties of the nanocomposite and provided a nanosubstrate that is suitable for neuronal studies, as well as increasing the hydrophilicity of the nanosubstrate. Using the nanoindentation method revealed a decrease in the stiffness of the nanosubstrate from 0.70 μN/nm to 0.49 μN/ nm after the coating of PANI-C, which represented a nanosubstrate with soft characteristics. The average ridge width (125 $\pm$ 94 nm) of nanogrooves changed the cells' native morphology to the elongated form by 51% and initiated further axonogenesis with an average length of 193$\pm$ 7 μm for each axon and an average number of 7 axons for each neurite. The combination of nanotopography and nanocomposite has synergistic effects on neuronal differentiation. The results of this study provided a platform for future cell therapy using differentiated neurons with functional axons. Although it is important to study the molecular pathway behind cellular differentiation by initiating mechanosensing in future studies.

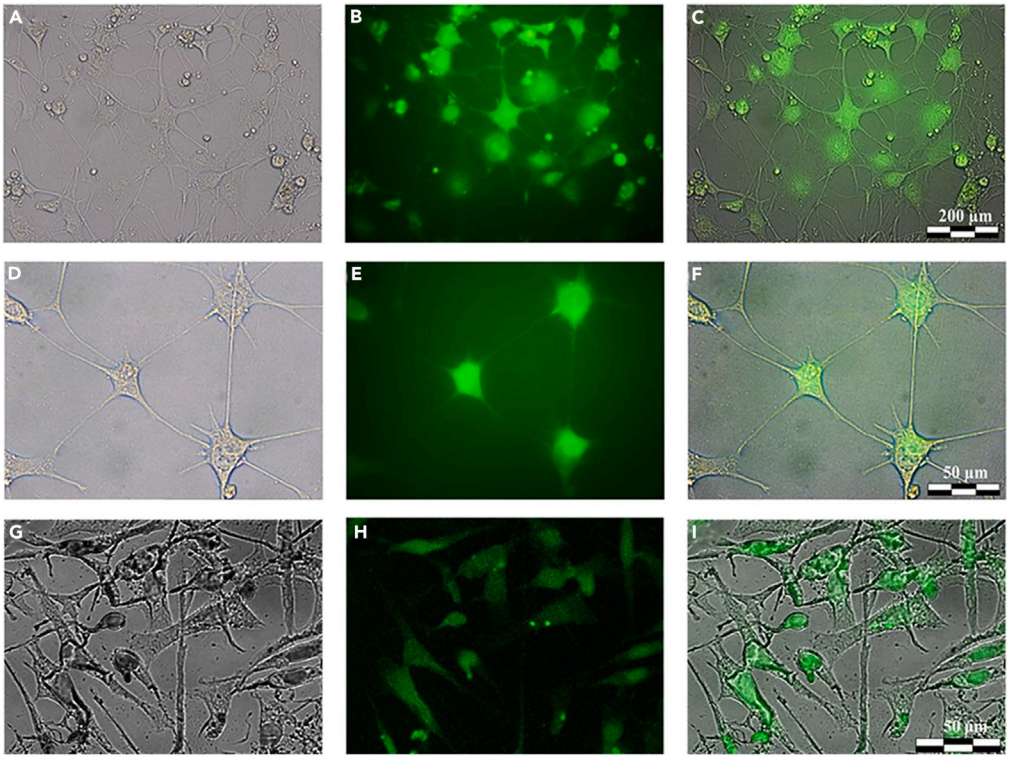

Figure 7. The fluorescent and confocal microscopy images of neurons differentiated from PC12 cells incubated with a primary antibody against neurofilaments and Alexa Fluor 488 as the secondary antibody

(A and D) The images were captured in phase contrast.

(B and E) Fluorescent microscopy images.

(C and F) Merged images of phase contrast and fluorescent microscopy images.

(G) The confocal light images of the positive control (PC12 cells treated with NGF).

(H) Fluorescent confocal image of the positive control.

(I) Merged images of light and fluorescent confocal microscopy images.

Limitations of the study

In this study, somatic cells werre differentiated into neurons by the combination of PANI-C and nanogroove topography. We investigated the cellular responses of the PC12 cell line to nanosubstrate with suitable physico-chemical properties. Hence, the molecular mechanism behind the neuronal differentiation via mechanosensing pathways on this nanosubstrate is not clear and requires further investigation. Moreover, the nanosubstrate exhibited inconsistencies on the microfluidic platform.

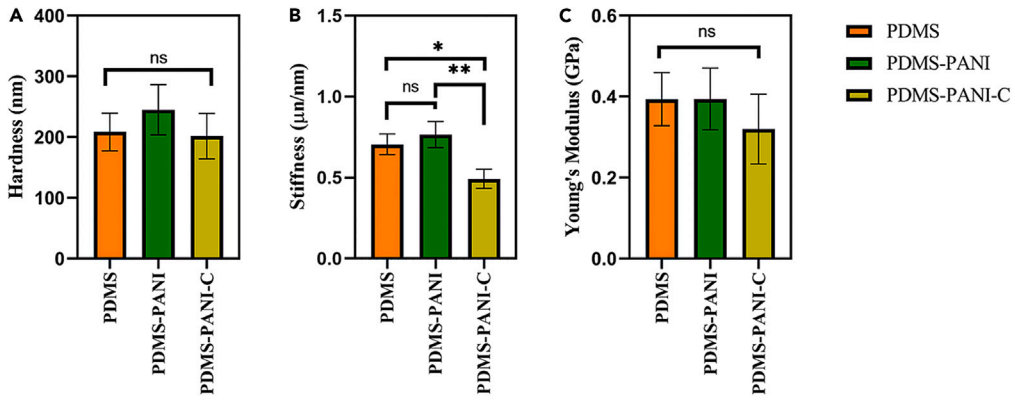

Figure 8. The mechanical properties of bare PDMS and PDMS coated with PANI and PANI-C nanosubstrates

(A) Hardness.

(B) Stiffness.

(C) Young's modulus.

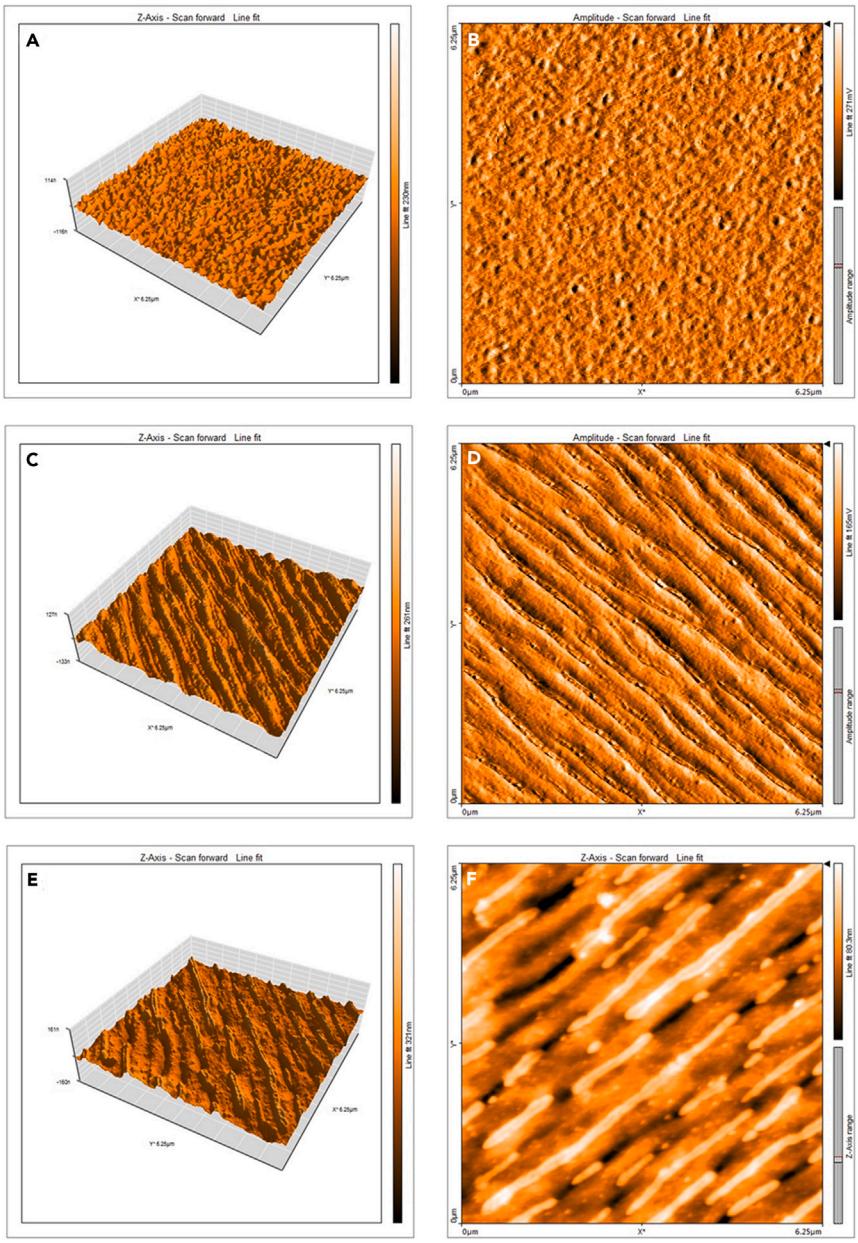

Figure 9. AFM topographic images

(A) 3D image of a flat PDMS substrate.

(B) 2D image of a flat PDMS substrate.

(C) 3D image of a nanogrooved PDMS substrate with a ridge width of 125 ± 94 nm.

(D) 2D image of nanogrooved PDMS substrate.

(E) 3D image of nanogrooved PDMS substrate coated with PANI-C.

(F) 2D image of nanogrooved PDMS substrate coated with PANI-C.

STAR★METHODS

Detailed methods are provided in the online version of this paper and include the following:

- KEY RESOURCES TABLE
- RESOURCE AVAILABILITY
  - Lead contact
  - Materials availability

SUPPLEMENTAL INFORMATION

Supplemental information can be found online at https://doi.org/10.1016/j.isci.2024.108828.

ACKNOWLEDGMENTS

The authors are thankful for funding from Iran National Science Foundation (INSF) grant No. 96006759. The authors also appreciate Ms. Yasaman Moazen Safaei for her corporation in this work.

AUTHOR CONTRIBUTIONS

Conceptualization: M.H.A., R.M., and A.A.
Investigation: M.H.A, R.M., H.S., S.J.
Analysis of data: M.H.A., R.M., A.A., H.S.
Writing original draft: M.H.A., R.M.
Review and editing: A.A. H.N-M.
Funding acquisition and supervision: A.A..

DECLARATION OF INTERESTS

The authors declare there is no conflict of interest.

Received: July 6, 2023
Revised: October 9, 2023
Accepted: January 3, 2024
Published: January 9, 2024

REFERENCES

1. Feigin, V.L., Abajobir, A.A., Abate, K.H., Abd-Allah, F., Abdulle, A.M., Abera, S.F., Abyu, G.Y., Ahmed, M.B., Aichour, A.N., Aichour, I., et al. (2017). Global, regional, and national burden of neurological disorders during 1990–2015: a systematic analysis for the Global Burden of Disease Study 2015. Lancet Neurol. *16*, 877–897.
2. Gerdts, J., Summers, D.W., Milbrandt, J., and DiAntonio, A. (2018). Axon self destruction: new links among SARM1, MAPKs, and NAD+ metabolism. Rev. del Col. Am. Cardiol. *72*, 2964–2979.
3. Mostafavi, E., Medina-Cruz, D., Kalantari, K., Taymoori, A., Soltantabar, P., and Webster, T.J. (2020). Electroconductive Nanobiomaterials for Tissue Engineering and Regenerative Medicine. Bioelectricity *2*, 120–149.
4. Yang, J., Wang, L., Huang, L., Che, X., Zhang, Z., Wang, C., Bai, L., Liu, P., Zhao, Y., Hu, X., et al. (2021). Receptor-targeting nanomaterials alleviate binge drinking-induced neurodegeneration as artificial neurotrophins. Explorations *1*, 61–74.
5. Shrestha, B.K., Mousa, H.M., Tiwari, A.P., Ko, S.W., Park, C.H., and Kim, C.S. (2016). Development of polyamide-6,6/chitosan electrospun hybrid nanofibrous scaffolds for tissue engineering application. Carbohydr. Polym. *148*, 107–114.
6. Kemkemer, R., Zenghao, Z., Linxiao, Y., Athanasopulu, K., Frey, K., Cui, Z., Su, H., and Luo, L. (2019). Surface modification of Polydimethylsiloxane by hydrogels for microfluidic applications. Curr. Dir. Biomed. Eng. *5*, 93–96.
7. Elnaggar, M.A., El-fawal, H.A.N., and Allam, N.K. (2021). Biocompatible PCL-nanofibers scaffold with immobilized fibronectin and laminin for neuronal tissue regeneration. Mater. Sci. Eng. C *119*, 111550.
8. Bakare, R.A., Bhan, C., and Raghavan, D. (2014). Synthesis and characterization of collagen grafted poly(hydroxybutyrate-valerate) (PHBV) scaffold for loading of

bovine serum albumin capped silver (Ag/BSA) nanoparticles in the potential use of tissue engineering application. Biomacromolecules *15*, 423–435.
9. Kulikouskaya, V.I., Paribok, I.V., Pinchuk, S.V., Kraskouski, A.N., Vasilevich, I.B., Matievski, K.A., Agabekov, V.E., and Volotovski, I.D. (2018). Polydimethylsiloxane Films Modified with Chitosan/Pectin Multilayers as Scaffolds for Mesenchymal Stem Cells. Appl. Biochem. Microbiol. *54*, 468–473.
10. Luo, J., Walker, M., Xiao, Y., Donnelly, H., Dalby, M.J., and Salmeron-Sanchez, M. (2022). The influence of nanotopography on cell behaviour through interactions with the extracellular matrix – A review. Bioact. Mater. *15*, 145–159.
11. Zheng, H., Tian, Y., Gao, Q., Yu, Y., Xia, X., Feng, Z., Dong, F., Wu, X., and Sui, L. (2020). Hierarchical Micro-Nano Topography Promotes Cell Adhesion and Osteogenic Differentiation via Integrin α2-PI3K-AKT Signaling Axis. Front. Bioeng. Biotechnol. *8*, 1–16.
12. Wu, C., Chin, C.S.M., Huang, Q., Chan, H.Y., Yu, X., Roy, V.A.L., and Li, W.J. (2021). Rapid nanomolding of nanotopography on flexible substrates to control muscle cell growth with enhanced maturation. Microsyst. Nanoeng. *7*, 89.
13. Chen, W., Han, S., Qian, W., Weng, S., Yang, H., Sun, Y., Villa-Diaz, L.G., Krebsbach, P.H., and Fu, J. (2018). Nanotopography regulates motor neuron differentiation of human pluripotent stem cells. Nanoscale *10*, 3556–3565.
14. Takagi, J., Petre, B.M., Walz, T., and Springer, T.A. (2002). Global conformational earrangements in integrin extracellular domains in outside-in and inside-out signaling. Cell *110*, 599–611.
15. Bastiaens, A., Xie, S., and Luttge, R. (2019). Nanogroove-enhanced hydrogel scaffolds for 3D neuronal cell culture: An easy access brain-on-chip model. Micromachines *10*, 638.
16. Yu, W., Gong, E., Liu, B., Zhou, L., Che, C., Hu, S., Zhang, Z., Liu, J., and Shi, J. (2023). Hydrogel-mediated drug delivery for treating stroke. Chin. Chem. Lett. *34*, 108205.
17. McNamara, L.E., Sjöström, T., Seunarine, K., Meek, R.D., Su, B., and Dalby, M.J. (2014). Investigation of the limits of nanoscale filopodial interactions. J. Tissue Eng. *5*, 2041731414536177.
18. Liu, J., Kim, Y.S., Richardson, C.E., Tom, A., Ramakrishnan, C., Birey, F., Katsumata, T., Chen, S., Wang, C., Wang, X., et al. (2020). Genetically targeted chemical assembly of functional materials in living cells, tissues, and animals. Genetica (The Hague) *367*, 1372–1376.
19. Vijayavenkataraman, S., Kannan, S., Cao, T., Fuh, J.Y.H., Sriram, G., and Lu, W.F. (2019). 3D-Printed PCL/PPy Conductive Scaffolds as Three-Dimensional Porous Nerve Guide Conduits (NGCs) for Peripheral Nerve Injury Repair. Front. Bioeng. Biotechnol. *7*, 266.
20. Richardson-Burns, S.M., Hendricks, J.L., Foster, B., Povlich, L.K., Kim, D.H., and Martin, D.C. (2007). Polymerization of the conducting polymer poly(3,4-ethylenedioxythiophene) (PEDOT) around living neural cells. Biomaterials *28*, 1539–1552.
21. Bramini, M., Alberini, G., Colombo, E., Chiacchiaretta, M., DiFrancesco, M.L., Maya-Vetencourt, J.F., Maragliano, L., Benfenati, F., and Cesca, F. (2018). Interfacing graphene-based materials with neural cells. Front. Syst. Neurosci. *12*, 12–22.
22. Humpolíček, P., Kašpárková, V., Pacherník, J., Stejskal, J., Bober, P., Capáková, Z., Radaszkiewicz, K.A., Junkar, I., and Lehocký, M. (2018). The biocompatibility of polyaniline and polypyrrole: A comparative study of their cytotoxicity, embryotoxicity and impurity profile. Mater. Sci. Eng. C *91*, 303–310.
23. Qazi, T.H., Rai, R., and Boccaccini, A.R. (2014). Tissue engineering of electrically responsive tissues using polyaniline based polymers: A review. Biomaterials *35*, 9068–9086.
24. Caponi, S., Mattana, S., Ricci, M., Sagini, K., Juarez-Hernandez, L.J., Jimenez-Garduño, A.M., Cornella, N., Pasquardini, L., Urbanelli, L., Sassi, P., et al. (2016). A multidisciplinary approach to study the functional properties of neuron-like cell models constituting a living bio-hybrid system: SH-SY5Y cells adhering to PANI substrate. AIP Adv. *6*.
25. Rahman, S.U., Bilal, S., and Ali Shah, A.U.H. (2020). Synthesis and characterization of polyaniline-chitosan patches with enhanced stability in physiological conditions. Polymers *12*, 1–13.
26. Khan, M., Husain, Q., and Ahmad, N. (2019). Elucidating the binding efficacy of β-galactosidase on polyaniline–chitosan nanocomposite and polyaniline–chitosan–silver nanocomposite: activity and molecular docking insights. J. Chem. Technol. Biotechnol. *94*, 837–849.
27. Eftekhari, B.S., Eskandari, M., Janmey, P.A., Samadikuchaksaraei, A., and Gholipourmalekabadi, M. (2021). Conductive chitosan/polyaniline hydrogel with cell-imprinted topography as a potential substrate for neural priming of adipose derived stem cells. RSC Adv. *11*, 15795–15807.
28. Moutsatsou, P., Coopman, K., and Georgiadou, S. (2017). Biocompatibility assessment of conducting PANI/chitosan nanofibers for wound healing applications. Polymers *9*.
29. Wiatrak, B., Kubis-Kubiak, A., Piwowar, A., and Barg, E. (2020). PC12 Cell Line: Cell Types, Coating of Culture Vessels, Differentiation and Other Culture Conditions. Cells *9*.
30. Cheng, H., Zhou, L., Li, B., Zhu, M., Too, H.P., and Choi, W.K. (2014). Nano-topology guided neurite outgrowth in PC12 cells is mediated by miRNAs. Nanomedicine *10*, 1871–1875.
31. Matsuzaki, Y., Maruta, R., Takaki, K., Kotani, E., Kato, Y., Yoshimura, R., Endo, Y., Whitty, C., Pernstich, C., Gandhi, R., et al. (2019). Sustained neurotrophin release from protein nanoparticles mediated by matrix metalloproteinases induces the alignment and differentiation of nerve cells. Biomolecules *9*, 510–513.
32. Yavuz, A.G., Uygun, A., and Bhethanabotla, V.R. (2009). Substituted polyaniline/chitosan composites : Synthesis and characterization. Carbohydr. Polym. *75*, 448–453.
33. Shao, W., Jamal, R., Xu, F., Ubul, A., and Abdiryim, T. (2012). The effect of a small amount of water on the structure and electrochemical properties of solid-state synthesized polyaniline. Materials *5*, 1811–1825.
34. Ajeel, K.I., and Kareem, Q.S. (2019). Synthesis and Characteristics of Polyaniline (PANI) Filled by Graphene (PANI/GR) nano-Films. J. Phys, Conf. Ser. *1234*, 012020.
35. Queiroz, M.F., Melo, K.R.T., Sabry, D.A., Sassaki, G.L., and Rocha, H.A.O. (2015). Does the use of chitosan contribute to oxalate kidney stone formation? Mar. Drugs *13*, 141–158.
36. Janaki, V., Oh, B.T., Shanthi, K., Lee, K.J., Ramasamy, A.K., and Kamala-kannan, S. (2012). Polyaniline/chitosan composite : An eco-friendly polymer for enhanced removal of dyes from aqueous solution. Synth. Met. *162*, 974–980.
37. Kumar, S., Dutta, P.K., and Koh, J. (2011). International Journal of Biological Macromolecules A physico-chemical and biological study of novel chitosan – chloroquinoline derivative for biomedical applications. Int. J. Biol. Macromol. *49*, 356–361.
38. Kumar, A., and Borah, B. (2021). Effect of plasma irradiation on biocompatibility and cell adhesion of polyaniline/chitosan nanocomposites towards Hep G2 and PBMC cells. Adv. Mater. Process. *1*, 146–155.
39. Gul, S., Shah, A.U.H.A., and Bilal, S. (2013). Synthesis and characterization of processable polyaniline salts. J. Phys, Conf. Ser. *439*, 012002.
40. Usman, F., Dennis, J.O., Ahmed, A.Y., Seong, K.C., Fen, Y.W., Sadrolhosseini, A.R., Meriaudeau, F., Kumar, P., and Ayodele, O.B. (2020). Structural characterization and optical constants of p-toluene sulfonic acid doped polyaniline and its composites of chitosan and reduced graphene-oxide. J. Mater. Res. Technol. *9*, 1468–1476.
41. Kotanen, C.N., Wilson, A.N., Dong, C., Dinu, C.Z., Justin, G.A., and Guiseppi-Elie, A. (2013). The effect of the physicochemical properties of bioactive electroconductive hydrogels on the growth and proliferation of attachment dependent cells. Biomaterials *34*, 6318–6327.
42. Nakajima, M., Ishimuro, T., Kato, K., Ko, I.K., Hirata, I., Arima, Y., and Iwata, H. (2007). Combinatorial protein display for the cell-based screening of biomaterials that direct neural stem cell differentiation. Biomaterials *28*, 1048–1060.
43. Abasi, S., Aggas, J.R., and Guiseppi-Elie, A. (2019). Permissive Electroconductive Nanocomposites for Neuronal Progenitor Cells. In International IEEE/EMBS Conference on Neural Engineering (NER (IEEE)), pp. 875–878.
44. Ferrari, A., Cecchini, M., Dhawan, A., Micera, S., Tonazzini, I., Stabile, R., Pisignano, D., and Beltram, F. (2011). Nanotopographic control of neuronal polarity. Nano Lett. *11*, 505–511.
45. Ferrari, A., Faraci, P., Cecchini, M., and Beltram, F. (2010). Biomaterials The effect of alternative neuronal differentiation pathways on PC12 cell adhesion and neurite alignment to nanogratings. Biomaterials *31*, 2565–2573.
46. Lin, Z., Yu, Z., and Wei, Y. (2020). Measurement of nanoindentation properties of polymers considering adhesion effects between AFM sharp indenter and material. J. Adhes. Sci. Technol. *34*, 1591–1608.
47. Valentová, H., and Stejskal, J. (2010). Mechanical properties of polyaniline. Synth. Met. *160*, 832–834.
48. Thanpitcha, T., Sirivat, A., Jamieson, A.M., and Rujiravanit, R. (2006). Preparation and characterization of polyaniline/chitosan blend film. Carbohydr. Polym. *64*, 560–568.
49. Gong, B., Zhang, X., Zahrani, A.A., Gao, W., Ma, G., Zhang, L., and Xue, J. (2022). Neural tissue engineering: From bioactive scaffolds and in situ monitoring to regeneration. Explorations *2*, 20210035.
50. Lu, J.Y., Zhu, Q.Y., Zhang, X.X., Zhang, F.R., Huang, W.T., Ding, X.Z., Xia, L.Q., Luo, H.Q.,

and Li, N.B. (2018). Directly repurposing waste optical discs with prefabricated nanogrooves as a platform for investigation of cell-substrate interactions and guiding neuronal growth. Ecotoxicol. Environ. Saf. *160*, 273–281.

51. Kang, K., Kim, M.H., Park, M., and Choi, I.S. (2014). Neurons on nanotopographies: Behavioral responses and biological implications. J. Nanosci. Nanotechnol. *14*, 513–521.
52. Shrestha, S., Jang, S.R., Shrestha, B.K., Park, C.H., and Kim, C.S. (2021). Engineering 2D approaches fibrous platform incorporating turmeric and polyaniline nanoparticles to predict the expression of βIII-Tubulin and TREK-1 through qRT-PCR to detect neuronal differentiation of PC12 cells. Mater. Sci. Eng. C *127*, 112176.
53. Ahsan, S.M., Thomas, M., Reddy, K.K., Sooraparaju, S.G., Asthana, A., and Bhatnagar, I. (2018). Chitosan as biomaterial in drug delivery and tissue engineering. Int. J. Biol. Macromol. *110*, 97–109.
54. Zhao, X., Li, P., Guo, B., and Ma, P.X. (2015). Antibacterial and conductive injectable hydrogels based on quaternized chitosan-graft-polyaniline/oxidized dextran for tissue engineering. Acta Biomater. *26*, 236–248.
55. Higuchi, A., Ling, Q.D., Chang, Y., Hsu, S.T., and Umezawa, A. (2013). Physical cues of biomaterials guide stem cell differentiation fate. Chem. Rev. *113*, 3297–3328.
56. Hoffman-Kim, D., Mitchel, J.A., and Bellamkonda, R.V. (2011). Topography, cell response, and nerve regeneration. Annu. Rev. *12*, 203–231.
57. Houchin-Ray, T., Swift, L.A., Jang, J.H., and Shea, L.D. (2007). Patterned PLG substrates for localized DNA delivery and directed neurite extension. Biomaterials *28*, 2603–2611.
58. Kim, S.M., Ueki, M., Ren, X., Akimoto, J., Sakai, Y., and Ito, Y. (2019). Micropatterned nanolayers immobilized with nerve growth factor for neurite formation of PC12 cells. Int. J. Nanomed. *14*, 7683–7694.
59. Xu, P., Hussain, A.M., Xu, X., Cui, J., Li, W., and Wang, G. (2010). Preparation and cytocompatibility of polyaniline/PLCL conductive nanofibers. In Proceedings - 2010 3rd International Conference on Biomedical Engineering and Informatics (BMEI), pp. 1719–1722.
60. Mahdavian, R., Hashemi, N., Sedghi, M., Soleymani, H., Vaezi, Z., and Naderi-Manesh, H. (2023). The role of a nanogrooved polydimethylsiloxane substrate on mesenchymal stem cells adhesion, self-renewing, and mechanical properties. Colloids Surfaces A Physicochem. Eng. Asp. *678*, 132506.
61. Babakhanova, G., Krieger, J., Li, B.X., Turiv, T., Kim, M.H., and Lavrentovich, O.D. (2020). Cell alignment by smectic liquid crystal elastomer coatings with nanogrooves. J. Biomed. Mater. Res. *108*, 1223–1230.
62. Sun, X., Hourwitz, M.J., Baker, E.M., Schmidt, B.U.S., Losert, W., and Fourkas, J.T. (2018). Replication of biocompatible, nanotopographic surfaces. Sci. Rep. *8*, 564–610.
63. Wang, W.Y., Pearson, A.T., Kutys, M.L., Choi, C.K., Wozniak, M.A., Baker, B.M., and Chen, C.S. (2018). Extracellular matrix alignment dictates the organization of focal adhesions and directs uniaxial cell migration. APL Bioeng. *2*, 046107.

STAR★METHODS

KEY RESOURCES TABLE

REAGENT or RESOURCE	SOURCE	IDENTIFIER
Antibodies		
Neurofilament Monoclonal Antibody	Elabscience	N/A
Goat anti-rabbit IgG-Alexa Flour 488	Elabscience	N/A
Chemicals, peptides, and recombinant proteins		
Fetal bovine serum (FBS)	Gibco, Thermo Fisher Scientific	Cat.# 26140079
Dulbecco's modified Eagle's medium (DMEM)	Gibco, Thermo Fisher Scientific	Lot.# 2383717
Chitosan	Sigma Aldrich	Cat.# 448869
MTT salt	Sigma Aldrich	Lot.# MKCK7253V
Ammonium persulfate	PanReac AppliChem	Cat.# A2146
Polydimethylsiloxane (PDMS)	Dow Corning SYLGARD™ 184	N/A
double-distilled deionized water (DDW)	Millipore-Q	N/A
HCl	Merck	N/A
H_2O_2	Merck	N/A
Aniline	Riedel-de Haën	Cat.# APP-9-012
Hoechst	Thermo Fisher Scientific	Cat.# H21492
Calcein AM	Thermo Fisher Scientific	Cat.# C1430
Nerve growth factor (NGF)	Invitrogen	Cat.# A42627
Experimental models: Cell lines		
PC12 cell line	Royan Institute (Tehran, Iran)	N/A
Software and algorithms		
GraphPad Prism	GraphPad	https://www.graphpad.com/
AtomicJ	NanoSurf	https://www.nanosurf.com/
ImageJ-Fiji	NIH	https://imagej.net/ij/

RESOURCE AVAILABILITY

Lead contact

Further information and requests for resources and reagents should be directed to and will be fulfilled by the lead contact, Abdollah Allahverdi (a-allahverdi@modares.ac.ir)

Materials availability

This study did not generate new unique reagents.

Data and code availability

- The raw data (microscopy, spectroscopy, and cellular analysis) will be shared by the lead contact upon request.
- This paper does not report original code.
- Any additional information required to reanalyze the data reported in this paper is available from the lead contact upon request.

EXPERIMENTAL MODEL AND STUDY PARTICIPANT DETAILS

Cell line maintenance and passaging

The PC12 pheochromocytoma cell line (Male rat, ATCC Number: CRL-1721) was purchased from the Royan Institute (Tehran, Iran) and cultured in DMEM with 10% FBS (Gibco, Thermo Fisher Scientific, Waltham, MA, USA) and 1% penicillin/streptomycin (Invitrogen). The cell culture flasks were stored in a humidified incubator at 37°C with 5% CO_2.

METHOD DETAILS

Synthesis of polyaniline (PANI)

In brief, ammonium persulfate and aniline monomer were separately dissolved in an aqueous HCl (Merck) solution (0.1 M).[59] All the reactions were conducted in an ice bath to prevent the exothermic reactions of the mixture. Then, the ammonium persulfate solution was added dropwise to the solution of anilinium chloride (Riedel-de Haën, Seelze, Germany) with a flow rate of 100 mL/h. The color of the final solution starts changing abruptly from light blue to dark green after a while. The reaction mixture was allowed to stir for 3 hours to form a greenish precipitant. The precipitant was centrifuged for 30 min at 5000 rpm and subsequently washed with dilute HCl, acetone, and DDW to remove unreacted monomers and oligomeric impurities. The final precipitant was stored and dried in the oven overnight at 65°C.

Synthesis of polyaniline-chitosan (PANI-C) nanocomposites

The synthesis of PANI-C nanocomposite was carried out based on Janaki et al.[36]'s method. 0.2 g Chitosan (Sigma Aldrich, Merck KGaA, Darmstadt, Germany) was dissolved in the proper amount of aqueous acetic acid (2 wt%) and stirred for 3 hours. In the next step, a 0.1 M aqueous solution of aniline monomer in HCl solution was added to the aqueous chitosan solution to form a homogenous mixture. 0.1M ammonium persulfate (PanReac AppliChem, Polígono Pla de la Bruguera, Barcelona, Spain) was added dropwise to the above mixture as an oxidant agent with vigorous stirring. The polymerization process was carried out for a day at room temperature. The color of the solution changes abruptly from dark blue to dark brown. After that, the mixture was centrifuged for 30 min at 5000 RPM and then washed as follows: with aqueous acetic acid (2 wt%), acetone, and DDW. The washing procedure was done several times. The precipitant was dried at 65°C overnight.

Characterization of PANI-C nanocomposite

The particle size, surface charge, and polydispersity index (PDI) of the nanocarriers were calculated by dynamic light scattering (Malvern Zeta Sizer 3000HS, Malvern, UK). Field emission scanning electron microscopy (FESEM) images of PANI-C nanocomposite were captured by Mira 3-XMU, Queensland, Australia. Fourier transform infrared (FTIR) spectroscopy was measured by the Bruker Tensor 27 Spectrometer, Bruker, Germany, and the XRD spectra were recorded by the Philips X'Pert MPD 40 kV, 40 mA, Cu, Amsterdam, Netherlands. UV-visible data was measured by the thermo-scientific NANODrop 2000/2000c (Waltham, Massachusetts, USA).

FESEM

In order to demonstrate both the morphology and the size of PANI-C nanocomposites, the FESEM (Mira 3-XMU, Queensland, Australia) was carried out. For this purpose, the PANI-C sample was turned into powder after the synthesis process. The samples were coated with a thin gold layer, and images were captured under low voltage and current conditions.

Fourier transform infrared spectroscopy (FT-IR)

FTIR spectroscopy (Bruker Tensor 27 Spectrometer, Bruker, Germany) was conducted to identify the functional group as well as the chemical bonding state in pure PANI, chitosan, and PANI-C. The solid samples were mixed with KBr salt at a concentration of 1% and ground to form a powder. Then, the samples were finely ground using the Nujol mulling technique to reduce scattering losses and absorption band distortions. The recorded spectra were evaluated in the range of 400–4000 cm^{-1} with a resolution of 2 cm^{-1}.

X-ray diffraction (XRD)

The XRD analysis of PANI and PANI-C was conducted to reveal the native crystalline spectra of pure PANI and the formation of possible crystalline structures after the presence of chitosan in the PANI-C synthesis process. The structural analysis of the sample was done by powder X-ray diffraction from 10° to 80°.

UV-Vis spectroscopy

Subsequently, sample solutions of PANI, PANI-C, and chitosan in N-Methyl-2-pyrrolidone (NMP), acetonitrile, and acetic acid (2%) (1 μg/1 mL) were prepared to initiate the intermolecular transitions. UV-Vis spectra of samples were recorded in the region 250–750 nm using the thermos-scientific NANODrop 2000/2000c (Waltham, Massachusetts, USA) spectrophotometer.

Fabrication of PDMS nanogroove

Fabrication of PDMS nanogroove was done as we described before.[60] The PDMS elastomer and cross-linker were mixed in a 10:1 w/w ratio and degassed for 30 minutes. Subsequently, the PDMS was poured on ultra-smooth glass and placed in an oven at 65°C overnight to cure the liquid PDMS and form it into solid PDMS sheets. Rectangular samples of approximately 2 × 7 cm were cut with a surgical blade. The samples were clamped from either end and stretched up to 30% of their primary length. As follows, the samples were plasma treated by the Harrick plasma cleaner PDC-32G-2 (Ithaca, New York, USA) for 1 min while uniaxial strain was applied. Finally, the sample was removed from the plasma chamber, and the applied strain was carefully removed to form the nanogrooves. The time of plasma treatment is a determining factor in the depth and frequency of nanogrooves.[36,59]

Mechanical characterization of the nanogrooves

The morphology and roughness of PDMS nanogrooves were characterized by AFM in non-contact mode. The nanogrooves were fabricated on PDMS sheets, as described in the previous section. The plasma treatment was carried out for 120 s, and then samples were placed on coverslip glass. A proper solution of PANI-C and PANI (45 μg/mL) was prepared and diluted in DDW to the final solution (45 ng/mL). It is important to use proper concentrations of nanocomposites during the procedure of coating PANI-C on nanogrooves. Hence, the final concentrations of PANI-C and PANI were diluted in DDW and dropped dropwise onto PDMS nanosubstrates to dry. Topography images of PDMS sheets were taken by CoreAFM (NanoSurf, Switzerland) in the tapping phase contrast mode. All the images and roughness analysis were processed by NanoSurf CoreAFM software. The elastic modulus and hardness of nanosubstrates, including PANI, PANI-C nanocomposites, and embedded nanogrooves, were measured by Nanoscope IV Koopa UV-1 (Koopa Pazhoohesh Company, Mazandaran, Iran).

Cell culture and sample preparation

The PC12 rat pheochromocytoma cell line was obtained from the Royan Institute (Tehran, Iran) and cultured in DMEM with 10% FBS and 1% penicillin/streptomycin (Invitrogen). The cell culture flasks were stored in a humidified incubator at 37°C with 5% CO_2.

Cytotoxicity and cell viability

The comparative cell viability of the PC12 cell line in the presence of different concentrations of PANI nanoparticles and PANI-C nanocomposites was investigated with tetrazolium dye. In this research, both PANI and PANI-C were used to investigate whether PANI-C exhibits less toxicity than PANI or not. After the cells reached a proper confluency, they were trypsinized, and 5000 cells were seeded in each well of a 96-well plate and placed in an incubator at 37°C and 5% CO_2 for 12 h. Then cells were treated with different concentrations of PANI and PANI-C (0, 30, 60, 90, 120, 150, and 200 μg/mL) and placed in the incubator. After 24 h, 48 h, and 72 h, the culture medium was removed and 100 μL of MTT solution (with a final concentration of 0.5 mg/mL) was added to each well for 2 h. After the treatment, DMSO was added to the wells in order to dissolve the formazan precipitates. The optical densities were measured at 570 nm using a microplate reader (BioTek Instruments, Inc., Winooski, Vermont, USA). For the MTT assay, three replicate tests were carried out for each concentration. The PC12 cell line without any treatment was considered the control group.

Characterizing cells' morphology

Previous studies reported that cells change their morphology and align parallel to the direction of nanogroove topography.[61–63] Hence, it is important to visualize cells' morphology in order to understand their behavior. Accordingly, 10,000 cells were seeded on PDMS nanosubstrate and placed in an incubator overnight to attach and form a decent morphology. The cells were then incubated for 2 hours with the final appropriate solutions of Calcein-AM/PI (10 μg/mL in HBSS) and Hoechst (10 μg/mL in PBS). All images were captured by the DP72 camera of the Olympus IX81 fluorescence microscope (Olympus Ltd., Tokyo, Japan).

Antibody staining and immunofluorescence assay

Immunofluorescence staining of the differentiated PC12 cells was performed using primary antibodies against Neurofilament68 (E-AB-33366) and E-AB-1055, and goat anti-rabbit IgG Alexa Fluor 488 was used as the secondary antibody. For this purpose, PC12 cells were cultured on PDMS sheets containing nanogrooves and PANI-C nanocomposites for two weeks. In order to immunoassay cells, the culture medium was discarded, and the samples were rinsed with PBS (37°C) several times. Then cells were incubated with paraformaldehyde (4%) and Triton X100 (1%) to become fixated and permeable. The primary antibodies were diluted to the proper dilution based on the manufacturing protocol and were used to stain the cells overnight. Following primary antibody treatment, the cells were washed several times with PBS and stained for 2 hours with an Alexa Fluor 488 secondary antibody. Finally, the cells were washed to remove the non-conjugated antibodies in order to eliminate possible background during microscopy. All cell images, including phase-contrast and fluorescent, were taken using an Olympus IX81 fluorescence microscope (Olympus Ltd., Tokyo, Japan).

QUANTIFICATION AND STATISTICAL ANALYSIS

We employed ImageJ-Fiji software (version 1.53c, Madison, WI, USA) to analyze images and quantify substrate properties and cell morphology. AFM force spectroscopic data were analyzed using AtomicJ. Statistical analysis, including analysis of variance (ANOVA) and mean comparison, was carried out using GraphPad Prism software (version 9.5.0).

ADDITIONAL RESOURCES

There are no other resources to declare.